Proceedings of the 21st ICSMGE, Vienna, Austria, 14 – 19 June 2026. Pistrol, Adam & Schweiger (eds.)
Published by: ÖGG, Austrian Society for Geomechanics, Salzburg, Austria, ISBN 978-3-9503898-4-5
https://doi.org/10.53243/ICSMGE2026-795

Simulation of the spread of destruction of overloaded columns in a road embankment – a case study

Waldemar Szajna
Institute of Civil Engineering, University of Zielona Góra, Poland, and TPA, Poland, w.szajna@ib.uz.zgora.pl

Liudmyla Bondareva
Department of Geotechnics, Kyiv National University of Construction and Architecture, Ukraine, and TPA, Poland

Bartosz Szatanik
Group of Engineering Geology and Geotechnics, TPA, Poland

ABSTRACT: The article presents the analyses of a low road embankment constructed on peat soil reinforced with drilled concrete displacement columns. The columns' bases were rested on the underlying sand layer. Due to significant uneven settlement of columns, the embankment and thus the road surface failed. Excessively wide column spacing caused their overloading. The analyses of the system were performed using a 2D finite element numerical model. The soil was modelled using the Hardening Soil and Mohr-Coulomb models. The model parameters were established based on CPTu and DMT tests. The subsequent phases of the simulation reflected the stages of embankment construction in terms of time. The columns were modelled as elastoplastic embedded beam elements, which failed under increasing loads. The authors used three methods of modelling the failure. In the first approach, column failure (yielding) was considered to occur when the normal stresses induced by bending reached the tensile or compressive strength of the concrete. In practice, however, tension dominated. The increase in load resulted in the propagation of yielding to the adjacent cross-sections of the column, creating the cracked segment. In the second modelling method, hinges were introduced at the points where the first yielding of the cross-section occurred, simulating a localized fracture. In the third method, the relevant column fragment was removed thus simulating shear damage. The degradation was sequential, starting from the outer columns, where the ratio of axial force to bending moment was the lowest, then progressed towards the central columns. Parametric studiers were performed, taking into account the method of modelling of the column failure as well as the involvement of the geotextile in the load transfer platform or the lack of such.

KEYWORDS: Embankment on columns, spread of failure, numerical simulation, parametric study.

1 INTRODUCTION

Modern roads are more and more frequently designed and constructed in areas of soft soils, e.g. peats. The construction of road embankments then requires the reinforcement of the subsoil. Various kinds of columns, such as drilled concrete displacement columns (DDC) or deep soil mixing columns (DSM), are very commonly used as reinforcement. Their function is to partially transfer loads from the embankment to the deeper, load-bearing subsoil layers. (Han, 2015) proposed a classification of columns based on installation method, material, and stiffness. The division according to the first two criteria is important for the execution of reinforcements and the functions they will perform in the system. For example, stone columns, in addition to carrying loads from the embankment, accelerate the consolidation of the soft soil. From the point of view of the mechanics of the system, the division according to stiffness is very important. Stone columns are regarded as flexible, DSM as semi-rigid and DDC as rigid.

The embankment is usually formed on a load transfer platform (LTP) reinforced with geosynthetic. In the triple-element system, i.e. LTP, a column and soft soil, the mechanism of load transfer is complicated (Han & Gabr 2002). It includes: the arching effect, the tensioned membrane effect, and stress concentration above the columns. The increase in the stiffness of the column, in relation to the stiffness of the soft soil, increases the so-called stress concentration factor, simultaneously raising the risk of damage to the system (Wehr et al. 2012).

Methods for modelling the interaction of system elements include: laboratory model tests, analytical formulations and numerical modelling. Kitazume & Maruyama (2006 & 2027) tested in a centrifuge model embankments on soft subsoil reinforced with DSM columns. Broms (2004) presented an analytical formulation of the column destruction mechanisms, the progressive nature of the phenomenon, and calculation methods for assessing its effects.

The numerical methods are dominated by 3D approaches, with the use of the Finite Element Method (FEM) or the Finite Difference Method (FDM). The Mohr-Coulomb (M-C) model, the critical state soil mechanics model (CSSM), and the Hardening Soil (HS) model were adopted as subsoil models. The M-C model was used in the works by Yapage et al. 2013, Jamsawang et al. 2016, Zheng et al. 2018, and Yu et al. 2021. The CSSM models were used in the publications by Chai et al. 2017 and Huang et al. 2020. The HS model was essential in the works by Gallant & Botero-Lopez 2021. The behaviour of columns' material in the cited works was simulated using various models, from linear elasticity, through the M-C model, to advanced damage plasticity models.

All presented methods of modelling the interaction of the embankment on columns with the subsoil indicate that the mechanisms of system destruction depend on the thickness of the soft layer. The main mechanism of destruction is related to the column fracture. However, they do not break simultaneously, but the process starts from the outer columns and progresses towards the centre. The bending moments in the columns are the greater, the lower is the subsoil strength and the smaller is the Area Replacement Ratio (*ARR*) measured as the ratio of the cross-sectional area of the columns to the horizontal cross-sectional area of the embankment base.

The paper analyses the case of a local road on a low embankment with a reinforced load transfer platform supported on concrete drilled displacement columns reinforcing the peat. Shortly after its commissioning, the road experienced significant uneven subsidence. The description of the failure and FEM numerical analyses of the system deformation (2D and 3D) are presented in Szajna et al. 2024. In this paper, the progressive nature of damage caused by column overloading is analysed. The aim of this work is to demonstrate the impact of

column fracture on the redistribution of internal forces and the behaviour of other components of the system. Due to the widespread use of 2D simulations in engineering design, the authors decided to formulate the problem in this form.

2 PROBLEM DESCRIPTION

The road crossing an area of peat soil, 5-6 m thick, was constructed on a low embankment (1.7 m) founded on concrete drilled displacement columns. The 0.3 m diameter columns were made of C16/20 concrete. The column spacing was 1.3 x 1.7 m, achieving ARR = 3.2%. The column bases were sunk into the underlying medium-density sand layer. A cross-section of the system is shown in Figure 1. The embankment rests on rows of columns, marked with symbols r. 1 ÷ r. 4. The columns were installed from a working platform on which an LTP reinforced with two layers of geotextile (EA = 1250 kN/m) was performed. The sequence of subsequent stages of construction is presented in Table 1.

Table 1. Construction stages description.

Stage	Description	Time [days]
1	Construction of working platform (0.5 m) + subsoil consolidation	60
2	Columns installation + soil consolidation	30
3	Bottom part of LTP (0.2 m) + consolidation	7
4	Bottom geotextile installation & construction of middle part of LTP (0.25 m) + consolidation	7
5	Upper geotextile + upper part of LTP (0.25 m) + consolidation	90
6	Pavement construction (0.5 m) + consolidation	7
7	Operating load (road – 5 kPa; sidewalk - 1.5 kPa)	-

Immediately after laying the asphalt surface, cracks appeared, and later, "egg carton"-shaped depressions occurred in the vicinity of the column heads. After five weeks, the differences in settlement in some depressions exceeded 20 mm and continued to progress.

The construction site was investigated by drilling, CPTu, and DMT. The results of these research, as well as laboratory tests, performed at the road design stage, were used to determine the soil parameters.

The results of parametric analyses presented in the work by Szajna et al. 2024 showed that the most probable cause of the failure could have been too low value of the Area Replacement Ratio. Also, the improper placement and the lack of geotextile pre-tension, reinforcing the LTP, could have resulted in too high a value of loads transferred directly to the soft subsoil, leading to its excessive deformation. Based on these observations, it is worth analysing how the overloading of the soft soil and the lack of the geotextile could have influenced the internal forces in the columns and their progressive damage.

3 NUMERICAL MODEL

Plaxis 2D was used to create the numerical model. The model dimensions, the element mesh, loads, and kinematic boundary conditions are presented in Figure 1. Although the real system does not show full symmetry with respect to the central vertical plane, it was assumed that such symmetry occurs in the model.

The analyses maintained the timelines for individual construction activities. To numerically represent them, the subsequent steps in Table 1 were converted into calculation phases. The term "stage" will refer to the construction steps, and the term "phase" to the numerical simulation steps. Almost each construction stage consists of a sequence of two phases in the model: a. plastic loading and b. consolidation. Thus, for example, phase 4b refers to consolidation in the fourth stage of construction, described in Table 1.

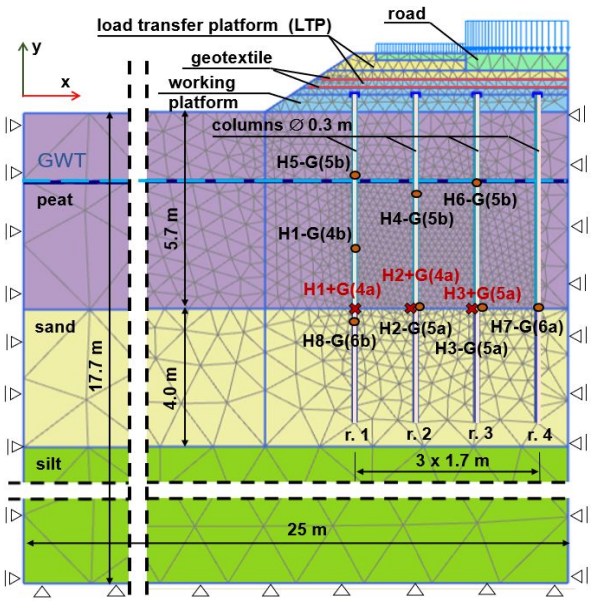

Figure 1. Basic finite element model.

The following constitutive models of the individual soil layers were used. The HS model was applied to simulate the behaviour of the subsoil layers. The model parameter values are listed in Table 2. The working platform and the LTP, which were made of sand, were simulated using the Mohr-Coulomb model, assuming the following parameter values: E = 25 and 40 MPa respectively and $\phi' = 33^0$ and $c' = 2$ kPa for both layers.

Table 2. Soil parameters.

Parameter	Peat	Sand	Silt
γ_{sat} [kN/m^3]	12.0	20.0	20.0
e_{init} [-]	3.00	0.50	0.75
E_{50}^{ref} [kN/m^2]	0.4	90.0	45.0
E_{oed}^{ref} [kN/m^2]	0.4	90.0	45.0
E_{ur}^{ref} [kN/m^2]	1.2	270.0	135.0
m [-]	0.7	0.5	0.6
ν [-]	0.2	0.2	0.2
c' [kPa]	7.0	0.0	5.0
φ' [°]	11.0	34.0	27.0
ψ' [°]	0.0	4.0	0.0
k_x [m/day]	0.01	15	0.005
k_y [m/day]	0.005	15	0.005
c_k [-]	1.500	0.250	0.375

The 2D approach and modelling columns as embedded beams are efficient in terms of model preparation time and computational time, but they are associated with certain limitations. First, the model geometry (plane strain) does not fully reflect the actual structure, as the columns are distributed discretely in the direction perpendicular to the analysis plane and experience 3D interactions with the surrounding soil. Second, the element exhibits some mesh dependency. Third, the ultimate load-bearing capacity of the column is not a result of the numerical analysis, but an input parameter to the model. Fortunately, the new element formulation (Smulders et al. 2019) reduces the first two unfavourable effects.

In the Plaxis 2D program, only three material models are available for embedded beam elements: elastic, elastoplastic

with constraints on tensile and compressive normal stresses in the beam cross-section, and elastoplastic with a moment-curvature relationship. In further analyses, the second of the above models was adopted. The cross-section yield condition in the tension and compression zones, respectively, is given by equations (1a) and (1b)

$$\left|\frac{N - N_{|Mp|}}{N_{tens} - N_{|Mp|}}\right| + \left|\frac{M}{M_p}\right| < 1, \text{if } N > N_{|Mp|} \quad (1a)$$

$$\left|\frac{N - N_{|Mp|}}{N_{comp} - N_{|Mp|}}\right| + \left|\frac{M}{M_p}\right| < 1, \text{if } N \leq N_{|Mp|} \quad (1b)$$

where: $N_{|Mp|}$ axial force for which the maximum bending moment can be obtained, M_p maximum bending moment, N_{tens} and N_{comp} are maximum tensile and compressive axial forces respectively.

For a circular column cross-section with a diameter of 0.3 m, made of C16/20 concrete, the shape of the asymmetric surface limiting elastic behaviour, in accordance with equations (1a) and (1b), is presented in Figure 2. The concrete parameters were adopted from Eurocode 2.

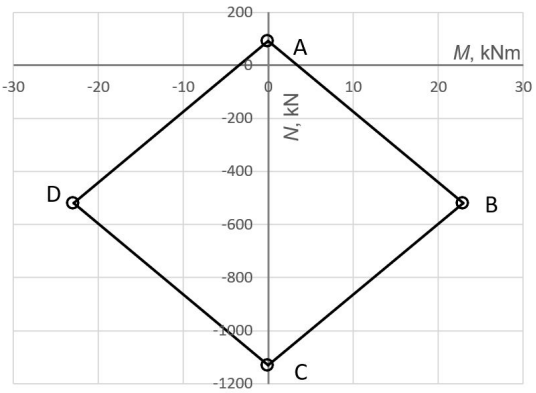

Figure 2. Envelope of limit cross-sectional forces of a C16/20 concrete column with a circular cross-section D = 0.3m (tension > 0).

The line segments AB and AD correspond to the limiting normal stresses in tension, while BC and CD correspond to the stresses in compression.

In the model used, at an established value of the axial force and an increasing bending moment, the extreme normal stresses in the column cross-section, can reach the strength of the concrete. In the case of tensile stresses, this corresponds to concrete cracking in the cross-section and it is the dominant mode of the columns destruction. With a further increase in the moment, this type of contractual destruction propagates to the adjacent cross-sections and the entire piece of the column model becomes cracked. In real concrete columns subjected to bending, a localized failure mode is more common. At the critical cross-section where the bending moment reaches its maximum value and a dominant crack develops in the tensile fibres, the column breaks. In a beam element, this type of failure can be modelled by a hinge. Finally, in an unreinforced concrete column cross-section, shear fracture may also occur as a result of the soft soil squeezing from under the embankment (Broms 2004). In such a case, the loaded upper part of the column no longer rests on the lower part, which is embedded in a strong subsoil. In this work, all three column damage models were used, but the shear damage model was used only for the first row of columns (r. 1) where the soil squeezing is the greatest. In each case, the force envelope from Figure 2 was used to determine the failure point. The hinge was modelled by reducing the stiffness of the relevant column section, and the shear fracture was modelled by removing it from the model.

The reinforced LTP is a crucial element in the load transfer system. Improperly deploying the geotextile, without removing the folds and pre-tensioning it, delays or prevents the reinforcement engagement. The analyses considered both full engagement of the geotextile and the lack of engagement.

4 ANALYSIS, RESULTS AND DISCUSSION

In order to facilitate the description of the variants of individual analyses and the models associated with them, abbreviated symbols are used, as described in Table 3. Symbols 1÷4 refer to the method of modelling the column destruction, while symbols 5 and 6 refer to the inclusion or omission of the geotextile, respectively. The symbol of the analysis type is followed by a symbol of engagement of the geotextile and the relevant phase number in parentheses, see Table 1 and Table 3. For example, the symbol H2-G(3b) denotes the hinged column model after the formation of the second hinge, without taking into account the geotextile, and the analysis was performed during the consolidation phase of the third construction stage.

Table 3. Analysis type designations.

No	Symbol	Model description
1	E	Elastic model of column
2	EP	Standard elastoplastic model of column
3	H*i*	Hinged column model with *i* hinge number
4	S1	Shear damage of the first column
5	+G	Active geotextile layer
6	-G	Inactive geotextile layer

In the following sections, analyses will be discussed taking into account the interaction of the geotextile and then in the absence of such interaction.

4.1 *The case of LTP with geotextile*

The comparison of the results of internal force analyses for individual models, it is worth starting with the axial force diagrams in the columns. The model type has little impact on the distribution of these forces. Figure 3 shows the force distributions in the external column r. 1 and the central column r. 4 (Figure 1). It is obvious that the smallest forces ($N_{max} \approx 50$ kN) occur at the edge of the embankment, and the largest ($N_{max} \approx 64$ kN) under its centre. The only exception is the case of shear damage of the first column (marked as S1) in which the force drops to several kN at the fracture point. This type of failure causes a slight increase in forces in adjacent columns.

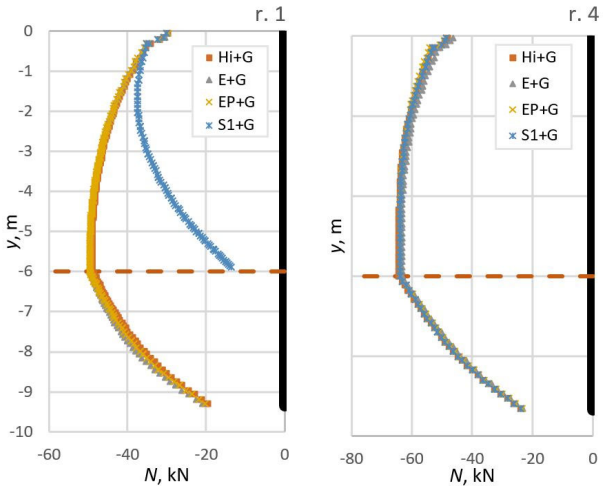

Figure 3. Influence of the model on the distribution of axial forces in columns: a) external (r. 1), central (r. 4) in the operational load phase.

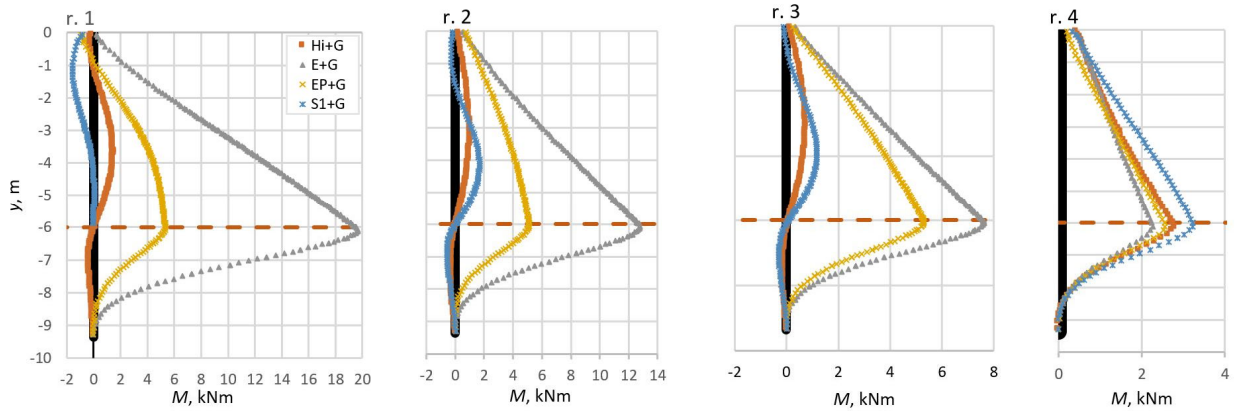

Figure 4. Bending moments in the operational load phase obtained for different column models, in columns r. 1 ÷ r. 4.

The ratio of the bending moment to the axial force (M/N) determines the failure of a column. However, since the axial forces are not very sensitive to the type of model adopted (except for the S1+G model), only the distributions of bending moments in the columns will be analysed in the following sections.

Figure 4 presents a summary of the bending moment diagrams obtained in the operational loading phase for individual column models. In the columns of the first three rows, the moments obtained for the elastic model (E+G) have the highest values. Concrete cannot withstand such high stresses in the tension zone and cracks. For example, in the first column, this value exceeds approximately four times the cracking (yielding) moment in the elastoplastic model (EP+G curve). In the hinged model (H*i*+G), the yield moment value necessitates the introduction of a hinge, and the bending moments are significantly reduced. Similarly, a shear damage reduces the moment. Here, however, the fibres begin to be intensively tensioned on the left side of the column system, at the top. In the second and third row of columns, changes occur in a similar way, but all moment values are lower than in the first column.

A different situation occurs in the central column (r. 4) near the embankment's axis of symmetry. From the point of view of concrete stress, the values of internal forces here are very favourable. The axial compressive forces are considerable, while the moments are significantly smaller than in the other columns. The bending moment values obtained from the elastic solution are lower than those obtained in the other models. In this case, the destruction of the outer columns causes a redistribution of internal forces and an increase in the load on the central column.

Moving on to the analysis of changes that occur at individual stages of the construction of the embankment, Figure 5 shows examples of moment distributions obtained for the model with hinges and with geotextile. Currently, in addition to the column model symbols and the geotextile activity symbol, the failure phase designation is given in parentheses. In Figure 5, in the first column (r. 1), the dominant moment diagram (marked H0+G(3b)) comes from the consolidation phase of the lower LTP layer. This is the phase preceding the fracture of columns r. 1 and r. 2. In the next phase (installation of the lower geotextile layer, symbol 4a, according to Table 1), as a result of the fracture of column r. 1, the first hinge is formed and the values of moments in this column decrease drastically (graph H1+G(4a)). At the same time, the moments in the remaining columns increase, leading to the fracture of column 2. The fracture of this column slightly increases the moments in columns 3 and 4. The consolidation phase (4b) does not cause further fractures. However, the installation of the top LTP layer and the top geotextile (phase 5a) leads to the fracture of column r. 3 and a significant increase in the moments in column r. 4 and a slight reduction in columns r. 1 and r. 2.

In summary of the analyses of the system with the interacting geotextile, it should be noted that the fractures of the subsequent columns in row 1, row 2, and row 3 occurred in the area of the top of the sand layer. The fracture locations are marked with red 'x' marks and red description in Figure 1.

4.2 *The case of LTP without geotextile*

If the geotextile is improperly deployed and inactive, the course and nature of column failure is different from the previously described. The description of the calculation phases still refers to the construction stages in Table 1, but the geotextile layers being installed are inactive.

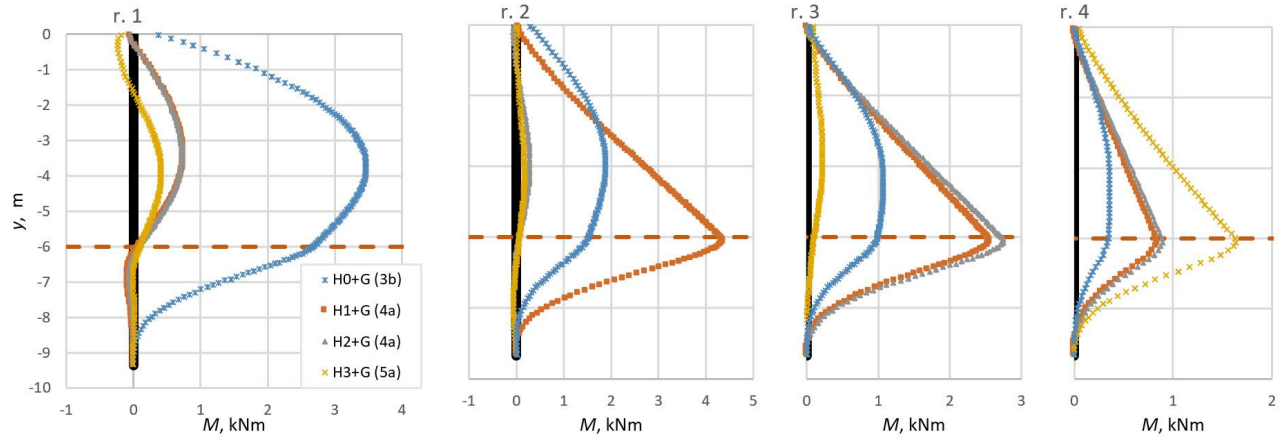

Figure 5. Bending moments in columns r. 1 ÷ r. 4, for the model with hinges obtained in subsequent stages of breaking.

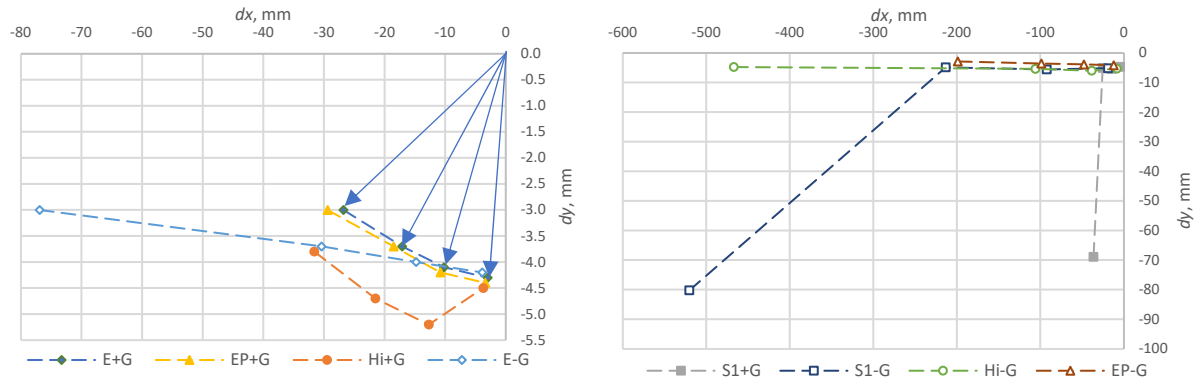

Figure 6. Comparison of relative displacements of column heads in models generating: a) small displacements, b) large displacements.

The subsequent fracture points of individual columns in the hinged model are marked in Figure 1 by orange dots with the description (-G). The first hinge was formed in the first column in phase 4b (consolidation of the lower part of the LTP). This time, however, the fracture occurred at a height of approximately one-third of the thickness of the soft layer, measured from its base. This point was marked as H1-G(4b). The next two fractures occurred in phase 5a. The second and third columns (r. 2 and r. 3) were fractured. In both cases, the breakage occurred in the sand top. A further three fractures occurred during the consolidation phase after the top layer of the LTP (5b) was installed. These fractures occurred in the first three columns, which had already failed, in the sequence r. 2, r. 1, and r. 3. This time, however, the hinges developed higher, near the groundwater level. The construction of the pavement structure (phase 6a) led to the fracture of the right column (r. 4). The failure occurred in the top of the sand layer. The final, eighth fracture, which affected column r. 1 for the third time, occurred during subsoil consolidation after pavement construction (phase 6b). The fracture occurred in the sand layer, at a depth of approximately 0.4 m from the top.

It is worth noting that some of the fractures occurred during the consolidation of the peat layer, during which the pore pressures were dissipated and the effective stresses increased.

4.3 *The influence of models on column heads displacement*

The presented analyses indicate that the method of modelling the destruction and the involvement of the geotextile significantly change the location of the fractures and the sequence of their formation. However, what is interesting is how this affects the embankment displacements. The basis for their assessment was the displacement distribution of the column heads supporting the entire structure.

Figure 6 shows the relative displacements of the column heads in relation to their original position. The significance of the individual results is explained by the vectors in Figure 6a for an exemplary elastic model with geotextile (E+G). Figure 6a shows the results obtained for models that generate small displacements, and Figure 6b shows those that generate large displacements. For clarity, the final vector positions, within a single model, are connected by thin dashed lines.

Figure 6a shows that the further out the column is located from the centre, the greater the horizontal displacements it experiences. For vertical displacements, the trend is reversed, except for the model with hinges (H*i*+G), in which the smallest settlements occurred in r. 4. The figure also shows that the absence of a geotextile results in large horizontal displacements. In the hinged (H*i*+G) model, the settlements in the fractured columns are significantly greater than those obtained for the EP+G model.

Figure 6b shows that large displacements occur in two cases. In the absence of a geotextile, large horizontal displacements occur (H*i*-G and EP-G models). Additionally shear damage is accompanied by large settlements (S1+G and S1-G).

5 CONCLUSIONS

The paper analyses the case of a low embankment placed on a peat layer reinforced with concrete displacement columns. The structure was characterized by a low degree of subsoil reinforcement (*ARR* = 3.2%). The embankment experienced significant deformation during construction. Besides the low *ARR* value contributing to column fracture, the probable cause of the failure may have been improper placement of the geotextile reinforcement. The geometry of the actual embankment was simplified by assuming that the system was symmetrical about a vertical plane passing through the centre of the road. To investigate possible causes of failure, a numerical analysis of the problem was performed by Plaxis 2D. In this version of the program, columns were modelled as embedded beam elements. The interaction of the geotextile in transferring loads was taken into account, as well as the scenario where the geotextile did not participate in the interaction. The failure of concrete columns was simulated using a linear-elastic model, an elastoplastic model, and a model in which a hinge was introduced in the yielded cross-section of the column. The case of failure of the outermost column in the form of shear damage at the point of yielding was also taken into account.

The computational models used allow the following conclusions to be drawn:

- Axial forces are insensitive to the assumed column material model. Their values are lowest in the outermost columns and increase as the columns are positioned closer to the embankment's axis of symmetry. The exception is the shear damage model, for which the force values decrease significantly after fracture.
- Adopting a linear-elastic model for concrete columns significantly overstates the bending moment values. If the geotextile is present, the moments in the elastic solution are four times higher than the value that causes the cross-section yielding.
- The elastoplastic model implemented in Plaxis 2D does not fully reflect the failure mode of concrete columns, although it limits the maximum values of bending moments.
- The attempt to model a localized column fracture using hinges requires manually identifying the phase at which the cross-section yields. Modifying the column's static

scheme by introducing a hinge was modelled by reducing the stiffness of the proper column section. It would be beneficial if the authors of the software introduced such functionalities into the Plaxis 2D code.

- The distributions of column bending moments are different during loading and consolidation phases. Column fracture can occur in either phase.
- Under heavy load on columns, when cross-sections are close to yielding, the system is very sensitive to small changes in parameters, including mesh dependency.
- The reinforcing layers of the geotextile play a significant role in load transfer. In the analysed case of the reinforced embankment three columns failed, while the columns in the unreinforced one fractured in eight places and in all four columns (the outermost column was damaged at three levels).
- The activation or lack thereof of the geotextile determines the occurrence of small or large horizontal displacements of the column heads. At the same time, column fracture with shear damage causes very large settlements of the heads.

The presented conclusions, formulated on the basis of a simplified concrete failure model, would require verification using more accurate models, e.g. the *Concrete mode*l in the Plaxis 3D.

6 REFERENCES

Broms, B.B. 2004. Lime and lime/cement columns. In *Ground Improvement* Ed. Moseley, M.P. and Kirsch, K. London. Spon Press, 252-330.

Chai, J., Shrestha, S., Hino, T., and Uchikoshi, T. 2017. Predicting bending failure of CDM columns under embankment loading. *Computers and Geotechnics* 91, 169-178.

Gallant, A.P., and Botero-Lopez, D. 2021. Lateral spreading and stability of embankments supported on fractured unreinforced high-modulus columns. *Deep Foundations Institute Journal* 15 (2), 1-21.

Han, J. 2015. Recent research and development of ground column technologies. *Ground Improvement* 168(GI4), 246-264.

Han, J. and Gabr M.A. 2002. Numerical analysis of geosynthetic reinforced and pile-supported earth platforms over soft soil. *Journal of Geotechnical and Geoenvironmental Engineering*, 128(1), 44–53.

Huang, Z., Ziotopoulou, K., and Filz, G.M. 2020. 3D numerical analyses of column-supported embankments: Failure heights, failure modes, and deformations. *Journal of Geotechnical and Geoenvironmental Engineering*, 146(12), 1–15.

Jamsawang, P., Yoobanpot, N., Thanasisathit, N., Voottipruex, P., and Jongpradist, P. 2016. Three-dimensional numerical analysis of a DCM column-supported highway embankment. *Computers and Geotechnics* 72, 42-56.

Kitazume, M., and Maruyama, K. 2006. External stability of group column type deep mixing improved ground under embankment. *Soils and Foundations* 46(3), 323–340.

Kitazume, M., and Maruyama, K. 2007. Internal stability of group column type deep mixing improved ground under embankment loading. *Soils and Foundations* 47(3), 437-455.

Smulders, C.M., Hosseini, S., and Brinkgreve, R.B.J. 2019. Improved embedded beam with interaction surface. *Proc. 17th Euro. Conf. on Soil Mech. & Geot. Eng*., Reykjavik, 1048–1055.

Szajna, W., Bondareva, L., and Szatanik, B. 2024. Analysis of deformations of road embankments founded on displacement columns improving soft subsoil. *Archives of Civil Engineering* 70(1), 19-36.

Wehr, J., Topolnicki, M., and Sondermann, W. 2012. Design risks of ground improvement methods including rigid inclusions. *ISSMGE - TC 211 Int. Symp. on Ground Improvement*, Brussels, Paper 35-22E, 1-9.

Yapage, N.N.S., Liyanapathirana, D.S., and Leo, C.J. 2013. Failure modes for geosynthetic reinforced column supported (GRCS) embankments. *Proc. 18th Int. Conf. on Soil Mech. & Geot. Eng*., Paris, 849-852.

Yu, X., Zheng, G., Zhou, H., and Chai J. 2021. Influence of geosynthetic reinforcement on the progressive failure of rigid columns under an embankment load. *Acta Geotechnica* 16, 3005-3012.

Zheng, G., Yang, X., Zhou, H., and Chai, J. 2018. Numerical modeling of progressive failure of rigid piles under embankment load. *Canadian Geotechnical Journal* 56(1), 23-34.

European Committee for Standardization, 2004. *EN 1997-2 Eurocode 2 Design of concrete structures - Part 1-1: General rules and rules for buildings*. Brussels: CEN.